Solid State Ionics 13 (1984) 191–203
North-Holland, Amsterdam

IONIC CONDUCTIVITY IN TYSONITE-TYPE SOLID SOLUTIONS $La_{1-x}Ba_xF_{3-x}$

A. ROOS, F.C.M. van de POL, R. KEIM and J. SCHOONMAN
Solid State Department, Physics Laboratory, Utrecht University, P.O. Box 80.000, 3508 TA Utrecht, The Netherlands

Received 15 December 1983

The ionic conductivity of single crystals of tysonite-type solid solutions $La_{1-x}Ba_xF_{3-x}$ ($0 \leq x \leq 0.095$) has been studied parallel and perpendicular to the crystallographic c axis in the temperature range 293–1300 K. Three regions can be discerned in the compositional dependence of the ionic conductivity: (i) the "pure" crystal, in which at room temperature no exchange occurs between different types of anion sites in the tysonite structure; (ii) an intermediate region ($0 < x < 7 \times 10^{-2}$) which reveals changes in both the conductivity activation enthalpy and the magnitude of the conductivity; (iii) a concentrated solid-solution region ($x > 7 \times 10^{-2}$), where fluoride ions interchange easily among the different anion sublattices. Diffusion coefficients calculated from ionic conductivity results, are in good agreement with those calculated from ^{19}F NMR measurements. Using the present data, along with ^{19}F NMR data, dielectric relaxation data and structural considerations, mechanisms governing the ionic conductivity are proposed.

1. Introduction

There have been many investigations on fast fluoride ion conductors. For solids with high fluoride ion conductivity a number of applications have been proposed, e.g. as electrode in a galvanic cell (ref. [1]), as solid membrane in a gas sensor [2] and as fluoride ion-selective electrode [3,4]. With the advance of microelectronic techniques to manufacture, for instance, ion-selective electrodes, a growing demand for suitable solid-state inner membrane contacts has emerged. Solid contacts are more compatible with microelectronic manufacturing techniques than the conventional solution contacts, and permit the construction of electrodes that can withstand high temperatures and pressures.

Fluorides with the fluorite (CaF_2) structure, e.g. alkaline-earth fluorides, and with the tysonite (LaF_3) structure, e.g. rare-earth (III) fluorides, exhibit relatively high fluoride ion conductivities. Especially fluorite-type solid solutions based on alkaline-earth fluorides have been studied extensively [5,6]. In previous studies performed in our laboratory, the ionic conductivity of fluorite-type solid solutions of alkaline-earth fluorides doped with LaF_3 or UF_4 has been investigated. It appears that in the concentrated region of these types of solid solutions a composition-independent amount of about one mole percent of interstitial fluoride ions with enhanced mobility, carries the current, the major fraction of the fluoride-excess being present in more or less extended defect clusters. In comparison with the fluorites there have been only a few studies of ionic transport in the tysonite-type fluorides. These materials deserve more attention, as the conductivities in, for instance, nominally pure LaF_3 and CeF_3, have been reported to be relatively high already at room temperature [7]. The current investigations were undertaken to elucidate the energetics and mechanisms for fluoride ion conduction in LaF_3 and the anion-deficient solid solutions $La_{1-x}Ba_xF_{3-x}$ ($0 \leq x \leq 0.095$). These materials are of particular interest, since their mechanism of ionic conductivity may be representative of the ionic trivalent halides with the tysonite structure.

Previous investigations of the electrical conductivity of LaF_3 [8–12] reveal clearly a lack of consistency in the ionic transport parameters. LaF_3, and its solid solutions are known to react with oxygen and water vapour at elevated temperatures. This can lead to the formation of oxygen-rich surface layers, which tend to mask the intrinsic conductivity [10]. Although there is still some disagreement concerning the exact crystal structure of LaF_3 [13], the weight of recent

evidence [14] favours a trigonal structure of space-group $P\bar{3}cl\text{-}D^4_{3d}$ in which there are three distinct fluoride sublattices. Anisotropic fluoride ion conductivity has been observed for undoped LaF_3 with $\sigma(\parallel c$ axis$) > \sigma(\perp c$ axis) (ref. [11]). It is generally believed that the intrinsic point defects in LaF_3 are thermally generated according to a Schottky mechanism, while the transference number for anions is unity.

This investigation reports on the ionic conductivity of single crystals of $La_{1-x}Ba_xF_{3-x}$ ($0 \leqslant x \leqslant 0.095$). The relevant defect parameters, characterizing the ionic transport, have been evaluated from the composition and temperature dependence of the ionic conductivity. Mechanisms for the ionic conduction processes are proposed. The dependence of the diffusion coefficients on the solute content is discussed.

2. Experimental aspects

Single crystals of $La_{1-x}Ba_xF_{3-x}$ ($0 \leqslant x \leqslant 0.095$) were grown by means of a modified Stockbarger crystal-growth method, using a R.F. heater and a nitrogen growth atmosphere. We employ a growing speed of 3 mm/h for these crystals. A detailed description of the equipment has been given before [15]. A $La_{1-x}U_xF_{3+x}$ ($x = 2.6 \times 10^{-3}$) crystal has been grown using the same growth method, employing a lowering speed of 6×10^{-2} m/h.

X-ray diffraction studies confirmed all the crystals to be single-phase with the LaF_3 ($P\bar{3}cl$) structure. Small pieces, perpendicular and parallel to the crystallographic c axis, were cut from the ingots. Sample dimensions are typically 3×10^{-2} m long and 9×10^{-3} m in diameter. The solute content of the studied samples was determined by neutron activation analysis. For one ingot, for which the nominal BaF_2 content was about 10 m/o, the radial as well as the axial distribution of the dopant concentration was determined. Within the accuracy of the analysis (3–6% in the obtained values) no radial distribution in the Ba concentration was found, while in the axial direction the Ba concentration increased from 7.93 m/o at the bottom, to 10.50 m/o at the top of the ingot, in accordance with the phase diagram [40].

As electrode contact materials a platinum paste (6082, Hanovia) or sputtered platinum electrodes (Edwards S150, sputter coater) were employed. No difference in conductivity properties of the crystals could be observed for these two contact materials. The samples were spring loaded between platinum disks in a nickel conductivity cell, capable of containing 4 samples at a time. The cell contained an ambient of nitrogen gas. This ambient gas was purified with two BTS (BASF) catalyst traps and two molecular sieve traps (Union Carbide), in order to minimize contact with oxygen and water vapour. The small-signal ac response of the samples was recorded for temperatures from 293 to 1300 K in the frequency range 10^{-2}–10^5 Hz, with a solartron frequency response analyser (1174). Bulk conductances were obtained from analysing complex plane representations of the recorded admittance parameters. A detailed analysis of the small-signal ac response studies is beyond the scope of the present study and will be reported elsewhere [16].

3. Results

The compositions of the studied samples as determined by neutron activation analysis are gathered in table 1. Fig. 1 presents the bulk ionic conductivity of nominally pure LaF_3, measured parallel and perpendicular to the crystallographic c axis. This figure reveals the ionic conductivity of the single crystals to be slightly anisotropic $\sigma(\parallel) > \sigma(\perp)$ up to about 415 K. The data for UF_4-doped LaF_3, measured perpendicular to the c axis have been included as well. At low and moderate temperatures, there is a small, but significant difference between the bulk ionic conductivity of pure and UF_4-doped LaF_3 since the conductivity decreases upon doping with UF_4. The chemical analyses of the nominally pure and UF_4 doped samples (table 1) indicate that the small decrease is due to compensation effects. The remaining BaF_2 content in the undoped sample is comparable to the actually incorporated amount of UF_4. At high temperatures the ionic conductivities of these samples coincide within the accuracy of the measurements.

The data in fig. 2a show the bulk ionic conductivity of several solid solutions $La_{1-x}Ba_xF_{3-x}$ ($\perp c$ axis) along with the data for pure LaF_3 ($\perp c$ axis). Fig. 2b represents the bulk ionic conductivity of the solid solutions $La_{1-x}Ba_xF_{3-x}$ ($\parallel c$ axis) along with the data for pure LaF_3 ($\parallel c$ axis). The conductivity values were

Table 1
Compositions in mole percent (m/o), and conductivity activation enthalpies of the solid-solution single crystals $La_{1-x}Ba_xF_{3-x}$.

Sample		$[BaF_2]$ (m/o) weighted	$[BaF_2]$ (m/o) analysed	ΔH_1 (eV)	ΔH_2 (eV)	ΔH_3 (eV)
1	⊥	nominally pure	<0.25	0.46 ± 0.02	0.26 ± 0.04	0.84 ± 0.06
2	∥	nominally pure	<0.25	0.43 ± 0.02	0.26	0.84
3	⊥	0.3	0.30	0.36 ± 0.03	0.23	0.58
4	∥	0.3	0.79	0.40	0.23	–
5	⊥	2.73	1.30	0.37	0.22	0.71
6	∥	2.73	2.10	0.38	0.29	–
7	⊥	5.0	7.10	0.38	0.25	0.74
8	⊥	7.8	9.52	0.37	0.27	0.53
9	∥	7.8	6.72	0.40	0.27	0.70
10	⊥	10.4	7.93	0.36	–	0.50
11	∥	10.4	8.56	0.36	–	–
12	⊥	2.5 m/o UF_4	0.26 [a]	0.45	0.26	0.77

[a] UF_4 analysis.

reproducible upon heating and cooling, unless the experiments were extended over periods of several weeks. In that case the conductivity data were lower upon cooling, probably due to the incorporation of oxygen and, thereafter, the formation of separate phases LaOF and La_2O_3 in the solid solutions $La_{1-x}Ba_xF_{3-x}$ The isothermal composition dependence (330 K) of the bulk ionic conductivity of the solid solutions is presented in fig. 3 and reveals a maximum for $x \simeq 0.07$. The isothermal conductivity curves at higher temperatures, e.g. 500 K and 900 K, exhibit a similar behaviour.

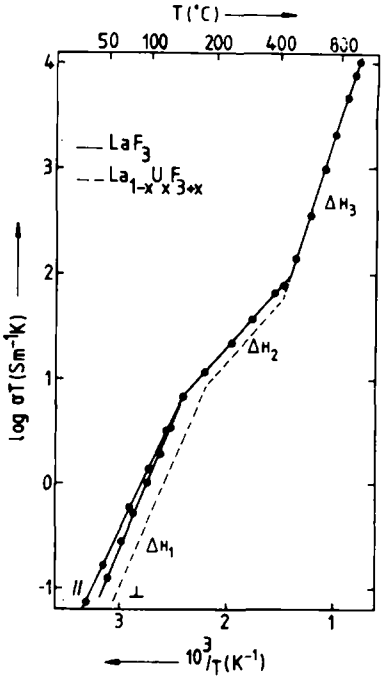

Fig. 1. The bulk ionic conductivity of LaF_3 (⊥ and ∥ c axis), and of $La_{1-x}U_xF_{3+x}$ ($x = 2.6 \times 10^{-3}$) ⊥ c axis.

The conductivity values as gathered in figs. 2a and 2b have been subjected to fitting to a sum of three exponential functions of the type $\sigma_i = \sigma_i^0/T \times \exp(-\Delta H_i/kT)$. The values for ΔH_i ranging from low to high doping levels, are gathered in table 1. Fig. 4 shows ΔH_i (⊥ c axis), plotted versus composition.

4. Crystal structure and possible conduction paths

In this section we review relevant literature data. For a long time the exact structure of LaF_3 was uncertain. Various papers are devoted to structural investigations of the tysonite-type minerals revealing a considerable amount of disagreement on the space group of these crystals [13]. Schlyter [17] has investigated the crystal structure of the natural mineral (La, Ce) F_3 and found the space group $P6_3/mmc$ with two formula units per unit cell. Mansmann [18] and Zalkin [19] could explain their structure inves-

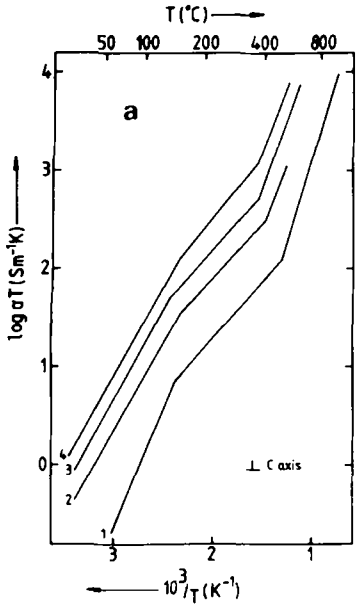

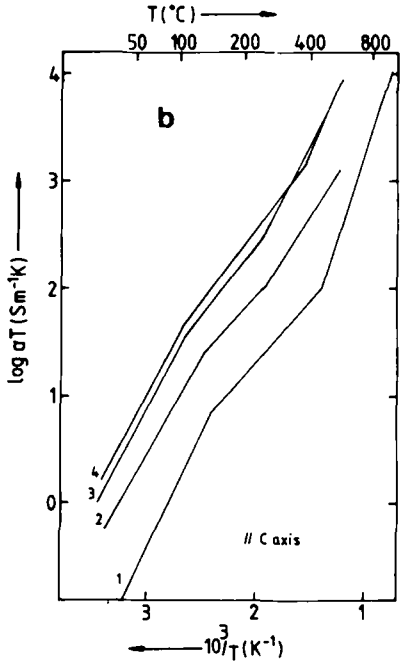

Fig. 2. The bulk ionic conductivity of pure LaF_3 and of several $La_{1-x}Ba_xF_{3-x}$ solid solutions: (a) ($\perp c$ axis): 1: $x = 0$, 2: $x = 3.00 \times 10^{-3}$, 3: $x = 1.30 \times 10^{-2}$, 4: $x = (7.1-9.52) \times 10^{-2}$. (b) ($\parallel c$ axis): 1: $x = 0$, 2: $x = 7.9 \times 10^{-3}$, 3: $x = 2.1 \times 10^{-2}$, 4: $x = (6.72-8.56) \times 10^{-2}$.

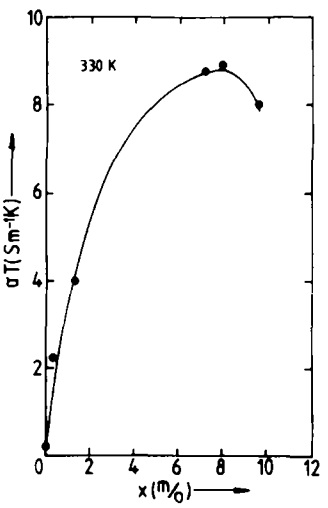

Fig. 3. The isothermal conductivity at 330 K plotted as σT versus x for the solid solutions $La_{1-x}Ba_xF_{3-x}$ ($\perp c$ axis).

tigations on LaF_3 with the trigonal space group $P\bar{3}c1$. This structure of LaF_3 was confirmed in a structure refinement with neutron powder data [20], and by recent investigations of Maximov and Schulz on pure LaF_3 used in this study [14]. All crystals grown for the present investigations, appeared to be single phase with the $P\bar{3}c1$-space group [15]. This structure is hexamolecular.

Thermal expansion measurements indicate the bulk volume to expand faster than the unit cell volume. This suggests that the thermal formation of point defects in LaF_3 occurs primarily by the Schottky mechanism [8]. Furthermore, calculations using structural data of LaF_3 [13], reveal that the interstitial sites (V_i^X) in LaF_3 allow ions with a radius up to 0.84 Å. This suggests that the occurrence of interstitial fluoride ions ($r = 1.19$ Å) is unlikely. In the fluorite-type solid solutions $Ba_{1-x}La_xF_{2+x}$ interstitial fluoride ions govern the conductivity. Here the interstitial sites allow ions with a radius of 1.43 Å. A lattice molecule situated at a one or more-dimensional lattice defect, needs to be taken into account in the thermal generation (or annihilation) of defects according to the Schottky mechanism. Hence the formation reaction can be represented by

$$La_{La}^X + 3F_F^X + V_{La}''' + 3V_F^{\bullet} \rightleftharpoons (LaF_3)_{defect} \cdot \qquad (1)$$

In the tysonite structure $P\bar{3}c1$ there are three in-

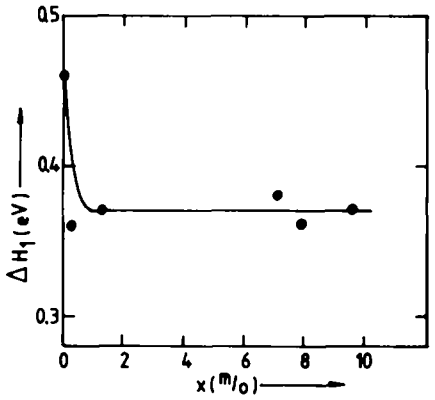

Fig. 4. The dependence of ΔH_1 on the composition parameter x for the solid solutions $La_{1-x}Ba_xF_{3-x}$ ($\perp c$ axis).

equivalent types of fluoride ion sites in the ratio 12:4:2 (F_1:F_2:F_3) (ref. [13]). However, two of these types of sites are almost equivalent ($F_2 = F_3$), and only two types need to be considered in the ratio 2:1 [F_1:($F_2 + F_3$)]. The F_1 type ions constitute the A sublattice and the F_2 and F_3 type ions constitute the B sublattice (see fig. 5). ^{19}F NMR measurements (ref. [21]) reveal that at room temperature the fluoride ions on one sublattice are moving much faster than those on the other sublattice, the concentration ratio of fast to slow being 1:2. This result indicates that only two types of fluoride ion sites need to be considered. According to recent structure investigations of pure LaF_3 [14], the $F_3 = F_2$ sites show positional disorder. Furthermore, the main diffusion path seems to run along the c axis [14]. This is in line with the observation that the conductivity along

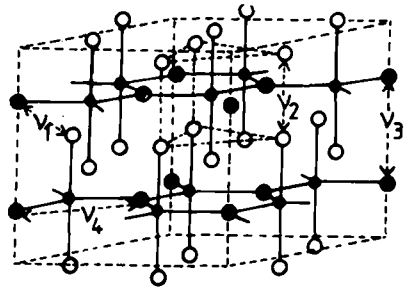

Fig. 5. Crystal structure of LaF_3 ($P\bar{3}c1$) and possible defect jumps. Black circles La, open circles F_1 and hatched circles F_2 and F_3. $a(F_1-F_2) = 2.5$ Å (ν_1), $a(F_1-F_1) = 2.5$ Å (ν_2), $a(F_2-F_2) = 3.68$ Å (ν_3), $a(F_2-F_2) = 4.15$ Å (ν_4).

the c axis exceeds that perpendicular to the c axis [11]. Powder neutron diffraction data obtained by Cheetham [22] reveal that the dopant BaF_2 generates vacant F_1 sites in a solid solution $La_{1-x}Ba_xF_{3-x}$. This would suggest that for the solid solutions the F_1 type ions are involved in the conduction paths.

The La^{3+} ions form a layered structure perpendicular to the c axis. Jaroszkiewicz and Strange [23] have proposed the three following conduction paths. The first defect jump with jump frequency ν_1 (see fig. 5) involves fluoride sites F_1 and F_2, and is a nearest-neighbour jump with distance a of 2.5 Å in directions predominantly in the ab plane, with a small component in the c direction. The second defect jump with frequency ν_2 involves F_1 sites only, and is a single jump along the c direction of about 2.5 Å. La^{3+} ions block further jumps in the same direction. The third defect jump with frequency ν_3 involves F_2 and F_3 sites only. The jump distance is 3.68 Å along the c direction (see fig. 5). Igel et al. [12] propose as the principal conduction path jumps between the F_2 type of sites, because these sites will be most energetically favourable. This defect jump with frequency ν_4 (jump distance of 4.15 Å) is in a direction perpendicular to the c axis only. They suggest further, that these jumps between F_2 sites may take place via a F_1 site, since the F_1-F_2 jump distances are rather short. However, this model is insufficient to explain the contribution parallel to the c axis at the intensity observed.

5. Discussion

A divalent cationic dopant (BaF_2) appears to increase, and a tetravalent cationic dopant (UF_4) appears to decrease the ionic conductivity of LaF_3 with respect to the nominally pure material. ^{19}F NMR investigations on LaF_3 show that fluoride ions are the migrating species [8,21,26]. As outlined before, Schottky defects are the most probable intrinsic point defects in LaF_3, and a vacancy mechanism for anion conduction is therefore most likely. The incorporation reaction for BaF_2 is then, under the assumption of substitutional replacement,

$$BaF_2 \rightarrow Ba'_{La} + V^{\bullet}_{F} + 2F^{\times}_{F} . \qquad (2)$$

The number of fluoride ion vacancies increases with BaF_2 concentration. The conductivity decreases with

a tetravalent dopant. The incorporation reaction for UF_4 can be represented by

$$3UF_4 \rightarrow 3U^{\bullet}_{La} + V'''_{La} + 12F^{\times}_{F} . \quad (3)$$

The increase of the concentration of lanthanum ion vacancies (V'''_{La}), causes a decrease of the extrinsic concentration of fluoride ion vacancies, and hence a decrease of the ionic conductivity. This is concordant with the results reported by Takahashi et al. [39] for the tysonite-type material CeF_3. They show that the conductivity of CeF_3 decreases upon doping with ThF_4, and increases upon incorporating for instance CaF_2.

Fielder [9] and Chadwick et al. [10] have studied undoped LaF_3. The results on the nominally pure sample in this study reveal fair agreement with their observations. Schoonman et al. [11] have measured single crystalline LaF_3 and polycrystalline ingots of the anion-deficient solid solutions $La_{1-x}Ba_xF_{3-x}$ ($0 \leqslant x \leqslant 0.1$). The present results on pure LaF_3 are in excellent agreement with these measurements. Our data match with the curves in ref. [11], and the activation enthalpies appear to be almost the same. The activation enthalpies for polycrystalline solid solutions as reported by Schoonman et al. [11] are higher than the values reported here. It should, however, be pointed out that due to grain boundary polarization effects the measurements on the polycrystalline solid solutions were limited to temperatures below room temperature. The present data were recorded well beyond room temperature. The enthalpies as obtained by TSDC (thermally stimulated depolarization current) and DL (dielectric loss) experiments, performed on our samples, are, as expected, in excellent agreement with the present conductivity data [27]. The data of Schoonman et al. [11] indicate a maximum to occur in the isothermal conductivity of the solid solutions for $x \simeq 0.05$. This tendency is also observed here. With regard to the compositional dependence of the bulk electrolyte conductivity, we distinguish the following development in the conduction mechanism: (i) the "pure" crystal, in which the conductivity at low temperatures is restricted to the B sublattice ($F_2 = F_3$): (ii) an intermediate region $0 < x < 7 \times 10^{-2}$, where exchange between the two different anion sublattices A and B increases together with an increase in the conductivity; (iii) a concentrated region for $x > 7 \times 10^{-2}$, where the fluoride ions exchange easily among the two sublattices, and where at low temperatures a percolation mechanism governs the conductivity.

5.1. "Pure" LaF_3 (samples 1 and 2)

Recent ^{19}F NMR measurements [25] reveal that at room temperature the F_2 (= F_3)-type ions (B sublattice) are moving faster than those of the F_1-type (A sublattice). In examining the crystal structure of LaF_3 (ref. [13]), we see that the jump distance ν_3 for the F_2-type ions is 3.68 Å along the c axis and 4.15 Å perpendicular to it, i.e. ν_4 (see fig. 5). As is well-known, the jump probability increases with decreasing jump distance. Furthermore, the activation enthalpy parallel to the c axis (0.43 eV) is smaller than the enthalpy perpendicular to this axis (0.46 eV). This agrees with the present result that below 415 K the ionic conductivity along the c axis exceeds that perpendicular to the c axis (fig. 1). Furthermore, the aforementioned structure investigations of pure LaF_3 [14] suggest the main diffusion path to be along the c axis via F_3-type sites. This should hold for the complete B sublattice. The temperature dependence of the ionic conductivities reveal slightly different activation enthalpies, i.e. ΔH_1 ($\parallel c$ axis) = 0.43 eV and ΔH_1 ($\perp c$ axis) = 0.46 eV. Above 415 K the anisotropy disappears, and the extrinsic ionic conductivity of LaF_3 reveals a knee (see fig. 1). Chadwick et al. [10] and more recently Igel et al. [12] propose as explanation for this phenomenon a classical changeover from a dissociation mode to a free-defect conduction mode (the so-called association model). However, Goldman and Shen [26] already reported an exchange of fluoride ions between inequivalent lattice sites to occur at 415 K. While recent NMR experiments [25] reveal their identification of the fast moving sublattice to be incorrect, the occurrence of exchange is essentially confirmed. Schoonman et al. [11] have employed the interchange model to account for the knee in the temperature dependence of the ionic conductivity of LaF_3. Their data on $La_{1-x}Ba_xF_{3-x}$ reveal the association model to be unlikely.

The diffusion coefficients calculated from ionic conductivity (D_σ) and ^{19}F NMR data (D_{NMR}) reveal good agreement, clearly indicating the absence of associates (see section 5.4). Furthermore, low-temperature dielectric relaxation measurements [27] indicate

that in nominally pure LaF_3 only 0.06 m/o divalent cations are present in impurity–vacancy associates. If this relatively small amount of divalent cations would be responsible for the appearance of the knee, at least 95% of these cations must be associated to a fluoride vacancy at room temperature. Although this depends on the equilibrium constant for association, such a large degree of association at 300 K is not very likely in view of D_σ being equal to D_{NMR}.

In a forthcoming study [16] we have analyzed the small-signal ac response of LaF_3 and the solid solutions. The data can be fit to an equivalent circuit, which includes the Debye circuit usually employed to model dipolar relaxation. However, the elements of the Debye circuit do not have the temperature dependence associated with dipolar reorientations, but rather the opposite, as is characteristic of the behaviour of free charge carriers. These results point also to a model wherein the conductivity is governed by one type of fluoride ions below 415 K along with a rapid exchange between the two anion sublattices above 415 K.

Recently, Franceschetti and Shipe [28] have developed a model for the small-signal ac response of ionically conducting materials with inequivalent lattice sites, which leads to a Debye-type of equivalent circuit. The model does not require the presence of dipolar complexes. In examining the tysonite structure one finds that in the direction of the c axis, and in the direction of the bisector of the a and b axis, the lattice planes occur in the pattern BAABAA, where "A" denotes a plane containing only F_1-type fluoride sites and "B" denotes a plane containing F_2- and F_3-type sites, here treated as equivalent. This situation is indicated schematically in fig. 6, where zero field transition probabilities P_0, P_1, P_2 and P_3 are indicated for the different possible jumps of anion vacancies between neighbouring lattice planes. The bulk small-signal ac response of LaF_3 has been calculated theoretically, using the standard thermally activated form for jump probabilities. Their analysis leads to the following equation for the high-frequency bulk resistance [28]

$$R_p = \frac{lkT}{e^2 c_0 A} \frac{(2 + P_2/P_1)}{a^2 P_0 + 2b^2(P_2 + 2P_3)}, \qquad (4)$$

where l is the thickness of the sample, c_0 the concentration of anion vacancies, A the cross sectional area, and a and b are the jump distances indicated in fig. 6. If we assume $P_3 = 0$, and make use of the jump frequencies and the activation enthalpies resulting from ^{19}F NMR experiments [25], we can calculate a theoretical Arrhenius-plot of the conductivity, $\log \sigma T$ versus $1/T$. The theory is in the present case not quantitative, and at best predicts the shape of the plot. It is nevertheless of interest to note that in pure LaF_3 the knee in the ionic conductivity cannot be reproduced by the theory when the jump frequencies and activation enthalpies derived from fits to the spin-lattice relaxation time in the rotating frame $T_{1\rho}$ (ref. [25]) are inserted. It appears that a much lower value for the exchange hopping time (originating from the spin–spin relaxation time T_2) is needed [24]. The enthalpy values ($\Delta H_1 = 0.46$ eV, $\Delta H_2 = 0.24$ eV) of the so-calculated conductivity curve (see fig. 7) resemble very well the values reported in this study (see table 1). Incidentally, this result suggests an important part of the $T_{1\rho}$ exchange frequency to originate from jumps that do not contribute to the conductivity process [25].

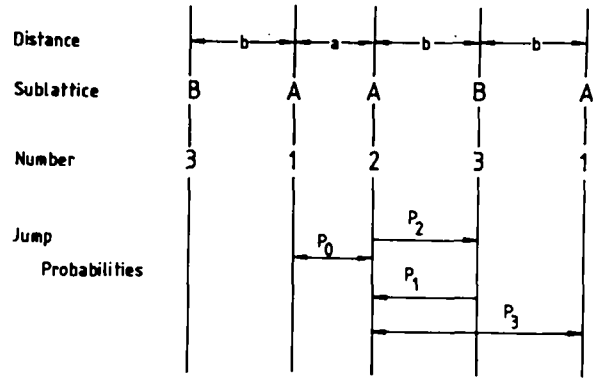

Fig. 6. Model used in calculating bulk ac response of tysonite-type materials. Vertical lines indicate lattice planes. Applied electric field is directed horizontally.

The enthalpy value ΔH_2 of the ionic conductivity of nominally pure LaF_3 between 415 and 715 K is 0.26 eV. This value reflects the conduction path energy barrier in the exchange conduction mode. The intrinsic region starts above 715 K with the value 0.84eV for the conductivity activation enthalpy ΔH_3 (see table 1). This value is in good agreement with the results from T_2 relaxation times [24] at low

temperatures, which lead to $\Delta H_{NMR}(T_2) = (0.84 \pm 0.04)$ eV. If we consider the value of 0.26 eV as the general migration enthalpy of fluoride ion vacancies, we obtain a value of (2.3 ± 0.3) eV for the Schottky disorder formation enthalpy ΔH_f. This value is in satisfactory agreement with the value 2.0 eV reported by Fielder [9] and the value 2.08 eV reported by Chadwick et al. [10].

5.2. Intermediate region: $0 < x < \simeq 7 \times 10^{-2}$ (samples 3–6)

In the intermediate region the ionic conductivity increases, and the activation enthalpy decreases with increasing dopant concentration (see figs. 3 and 4). An increase in added BaF_2-concentration from 0 to 0.3 m/o results in an increase of the ionic conductivity by a factor of about 10, and a decrease of ΔH_1 ($\perp c$ axis) from 0.46 to 0.36 eV. The bulk ionic conductivity shows again a knee. Within the experimental error, the migration enthalpy ($\Delta H_2 = 0.23$ eV) is comparable with the value obtained for the undoped material. Above approximately $\simeq$625 K, we can recognize in curve 2 in fig. 2 the usual increasing contribution of the intrinsic conductivity to the total conductivity. At first glance, a change-over from extrinsic to intrinsic conductivity seems inadequate to account for the conductivity rise in the more concentrated solid solutions beyond 625 K. However, due to defect–defect interactions between for instance V'''_{La} and $V^{\bullet}_{F}$, which lower the formation enthalpy, thermal defect densities will increase with increasing solute content.

We will discuss again the knee at $\simeq$415 K in view of two models, i.e. the association model, and the exchange model. When we first consider the association model [29], the isothermal conductivity is expected to vary proportional to $(x)^{1/2}$, x being the dopant concentration. It appears that the isothermal conductivity is proportional to $(x)^{1/2}$ for temperatures not only below 415 K, but also in the exchange mode, and the intrinsic conductivity region. This is not to be expected from the association model [29].

Let us accept that the isothermal conductivity below 415 K meets the $(x)^{1/2}$ requirement and consider the consequences of the association model. The ideal solution approximation, which ignores coulombic interactions between defects, is formally not applicable for moderate dopant concentrations ($x > 1 \times 10^{-3}$). The degree of association can be lowered by taking into account interactions between the free defect ($V^{\bullet}_{F}$), and its surrounding charge-cloud, the so-called Debye–Hückel–Lidiard (DHL) theory [30]. The reduction of the association enthalpy can then be interpreted as a change-over from conductivity in the association region at low doping concentrations to a new free-defect conductivity in the concentrated region. By applying the DHL theory, the decrease of the association enthalpy can be calculated,

$$\Delta H_A = \Delta H^0_A - \frac{q^2\kappa}{4\pi\epsilon\epsilon_0(1 + \kappa R)} \tag{5}$$

with

$$\kappa = (2q^2 X_c / V\epsilon\epsilon_0 kT)^{1/2} , \tag{6}$$

where κ is the Debye–Hückel screening constant, R the distance of closest approach for the free defect, i.e. the Ba'_{La}–$V^{\bullet}_{F}$ distance following the nearest-neighbour (nn) separation, V the volume per molecule LaF_3, X_c the free charged-defect concentration. The other parameters have their usual meanings. We can calculate, according to this relation, the lowering of ΔH_A for the solid solutions $La_{1-x}Ba_xF_{3-x}$. ΔH_A is lowered by about 0.15 eV for $X_c = 3 \times 10^{-3}$, and by 0.25 eV for $X_c = 2.10 \times 10^{-2}$. When we accept tentatively 0.46 eV ($= \Delta H_1$) of the pure material as the summation of the migration enthalpy and half of the association enthalpy for dilute systems, we can calculate using eqs. (5) and (6) the expected ΔH_1 values of the solid solutions. For the 0.3 m/o ($\perp$), and the 2.1 m/o ($\parallel$) doped sample we find 0.39 eV and 0.34 eV for ΔH_1, respectively. While the activation enthalpy of the 0.3 m/o doped sample is in reasonable agreement with the experimental value of 0.36 eV, the value found for the 2.10 m/o doped sample is too low compared with the experimental value of 0.38 eV. Especially because the conductivity activation enthalpy (ΔH_1) is practically solute independent for all solid solutions (see fig. 4), we conclude that the association model fails to describe satisfactorily our experimental results.

On the other hand, the aforementioned exchange model of Franceschetti and Shipe [28] can be used to describe the experimental observations adequately. With $P_3 = 0$ and the NMR values for jump frequencies and activation enthalpies [24,25], we have

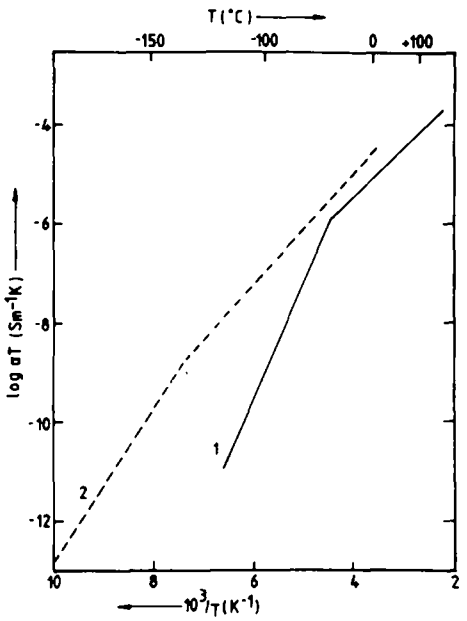

Fig. 7. The bulk ionic conductivity of pure LaF_3 (1), and of $La_{1-x}Ba_xF_{3-x}$ ($x = 3.00 \times 10^{-3}$) (2), computed from R_p, eq. (4), with parameters given in the text.

calculated a theoretical log σT versus $1/T$ plot (see fig. 7). It appears that the theoretical ionic conductivity reveals again a knee. Furthermore, the plot reveals that for the parameters used the knee, and hence the onset of defect exchange between the sublattices, moves towards lower temperatures, compared to the pure material. This trend stems from ^{19}F NMR measurements [24], where a maximum shift of about 60° was observed. The shift of the knee is in qualitative agreement with the curves in fig. 2a and b. While at higher defect concentrations the exchange sets in at lower temperatures, the defect jumps may be partly of a local nature. We suppose them to occur near the dopant ions, so that they do not contribute to ionic transport. This local relaxation can be observed in the NMR measurements. Therefore, the present discussion cannot be raised beyond a qualitative comparison. The theoretical conductivity curve leads for the 0.3 m/o doped sample to a value of 0.34 eV for ΔH_1, and this value is lower than the enthalpy value of 0.46 eV for pure LaF_3. The enthalpy value (ΔH_2) of the calculated curve above the knee remains nearly unchanged for undoped and doped LaF_3 (0.3 m/o), i.e. 0.24 eV and 0.23 eV, respectively.

^{19}F NMR studies [24,25] reported that the onset of the exchange is not shifting further to lower temperatures for solute contents, higher than 0.9 m/o. This could explain the absence of a decrease in ΔH_1 for the solid solutions. In conclusion, the average enthalpy value below 415 K ($\Delta H_1 = 0.37$ eV $\perp c$ axis) is a consequence of the migration of fluoride ion vacancies through the B sublattice.

5.3. Concentrated region: $x > \simeq 7 \times 10^{-2}$ (samples 7–11)

For the highest solute levels, up to the limiting BaF_2 concentration for which the tysonite structure is preserved, the values for the activation enthalpies remain approximately constant with increasing solute content (see table 1). The isothermal conductivity reaches a maximum for a composition with about 7 m/o dopant (see fig. 3), and is slightly lower for the 9.5 m/o sample. It is noted that at about 7 m/o minimum occurs in the fluorine–fluorine correlation times of the solid solutions $La_{1-x}Ba_xF_{3-x}$ determined by ^{19}F NMR (ref. [25]). This decomposition dependence has been reported also by Takahashi et al. [39] for tysonite-type solid solutions $Ce_{1-x}Ba_xF_{3-x}$. Here the maximum conductivity occurs at about 5 m/o BaF_2 (ref. [39]). In examining the curves for high solute contents >7 m/o, one finds that the distinction between the migration enthalpy in sublattice B, and the migration enthalpy in the exchange mode fades away. Further, the conductivity anisotropy disappears for the concentrated solid solutions. This, in conjunction with the fading away of the knee in the Arrhenius plots, points to an enhancement of the exchange between the sublattices with increasing dopant concentration along with the occupation of F_1 positions by vacancies. This is confirmed by a structure analysis which shows a dilation along the c axis with increasing composition parameter x (ref. [15]), and by measurements of the spin–spin relaxation time T_2 (ref. [24]), which show activated behaviour on F_1-type sites to occur for increasing dopant concentration. Further confirmation is found in the powder neutron diffraction experiments by Cheetham [22], which could be interpreted assuming that the dopant BaF_2 generates vacant F_1 sites in the solid solution $La_{1-x}Ba_xF_{3-x}$.

Upon increasing the solute content in the concentrated region, the effects are solute independent ac-

tivation enthalpies ΔH_1 and ΔH_2, pre-exponential factors, and ionic conductivities. We can explain these phenomena by assuming that the conductivity in these solid solutions is governed by a percolation mechanism. In this respect the present solid solutions compare well with a number of well-known solid electrolytes such as ZrO_2, stabilized by incorporation of aliovalent oxides CaO and Y_2O_3. These fluorite-type solid solutions reveal a high ionic conductivity due to a high oxygen vacancy concentration. Numerous experimental works (refs. [31,32], and references therein) on the ionic conductivity of these systems, have shown that these compounds exhibit also a maximum in the conductivity isotherms. For example, in calcia-stabilized zirconia, $Zr_{1-x}Ca_xO_{2-x}$, the maximum occurs around 13 m/o calcia and it appears that the position of the maximum can be explained with a percolation mechanism [31].

Now we shall discuss the percolation mechanism [33], which can explain indeed the saturation in the bulk ionic conductivity of the concentrated solid solutions $La_{1-x}Ba_xF_{3-x}$. Since the fluoride ion vacancies are the charge carriers, dc ionic conductivity can arise only when the vacancies can migrate without hindrance through the specimen. This will be realized if two conditions are satisfied: (i) Randomly distributed impurity ions form chains linking infinitely remote points in the specimen. (ii) The probability of realization of such chains is finite. The chains form conduction paths along which vacancies can migrate. The formulation of the problem is not altered if we assume that vacancies can migrate only between the nearest- and next-nearest-neighbour anion sites near Ba'_{La} ions. In other words, $(Ba_{La}V_F)^X$ associates, and nearby isolated Ba'_{La} defects provide a dc conduction path, for which dissociation need not be taken into account.

From the theory it is known [34] that the probability of formation of infinite chains of nearest-neighbour impurity atoms randomly distributed in a crystal, becomes finite only when the impurity atoms reach a critical concentration x_t. This threshold concentration is called the percolation limit. From this point of view we should expect to find a maximum in the ionic conductivity in the system on attainment of the threshold concentration x_t of impurity atoms. It can be calculated that the percolation threshold for a continuous nn → nn conduction path in LaF_3 is achieved for 6.7 m/o BaF_2. When we assume that also jumps are possible from nn → nnn positions, the percolation threshold is achieved for 2.7 m/o BaF_2. The concentration dependence of the conductivity for $La_{1-x}Ba_xF_{3-x}$ (fig. 3), indicates that for this system the percolation threshold is achieved at ≃7 m/o BaF_2. This is in accordance with a percolation threshold for a nn → nn conduction path.

5.4. Pre-exponential factor

Using the pre-exponential factors (σ_1^0), we can calculate the fluoride ion diffusion coefficients for pure LaF_3, and the solid solutions $La_{1-x}Ba_xF_{3-x}$. These diffusion coefficients can be calculated from the ionic conductivity results via the macroscopic Nernst–Einstein equation:

$$\sigma T = Nq^2D/k \tag{7}$$

and

$$D = \nu_0 a^2 g \exp(\Delta S_m/k) \exp(-\Delta H_m/kT)\,, \tag{8}$$

where N is the number of anions per unit volume, a the jump distance, D the diffusion coefficient, ν_0 an effective vibrational frequency usually equated to the Debye frequency [$\nu_0 = 7.5 \times 10^{12}$ s^{-1} (ref. [8]), g a structure and symmetry factor, and ΔS_m and ΔH_m the entropy and enthalpy of motion, respectively. The other parameters have their usual meanings. The calculated diffusion coefficients (D_σ) are gathered in table 2. The diffusion coefficients obtained in this way may be compared with those derived from ^{19}F NMR relaxation measurements, (ref. [24]). Since both sets of experiments were performed on the same samples, variation in sample characteristics are eliminated. The diffusion coefficients can be evaluated from the NMR results via the Einstein equation [9], i.e.

$$D_{NMR} = \nu a^2 g\,, \tag{9}$$

where ν is the jump frequency. D_{NMR} values are included in table 2, and have been calculated only for directions perpendicular to the c axis, because the NMR technique does not distinguish between jumps perpendicular and parallel to the c axis. At room temperature the ionic motion takes place through the anion B sublattice. For the calculations perpendicular

Table 2
Diffusion coefficients at 300 K calculated from conductivity (D_σ) and ^{19}F NMR (D_{NMR}) data (ref. [24]), and migration entropies for nominally pure LaF_3 and the solid solutions $La_{1-x}Ba_xF_{3-x}$.

Sample		[BaF_2] (m/o)	D_σ (10^{-14} m^2 s^{-1})	D_{NMR} (10^{-14} m^2 s^{-1})	$\Delta S_m/k$
1	⊥	nominally pure	0.26 ± 0.09	0.26 ± 0.02 a)	−1.5 ± 0.4
2	∥	<0.25	0.23 ± 0.07	–	−1.5
3	⊥	0.3	1.8 ± 0.6	4.4 ± 0.4	−2.3
4	∥	0.79	3.3 ± 1.1	–	−3.3
5	⊥	1.30	2.4 ± 0.8	–	−2.8
6	∥	2.10	4.6 ± 1.5	–	−2.3
7	⊥	7.10	5.8 ± 1.9	8.3 ± 0.8	−2.8
8	⊥	9.52	5.7 ± 1.9	–	−2.6
9	∥	6.72	5.6 ± 1.9	–	−2.5
10	⊥	7.93	4.7 ± 1.6	4.6 ± 0.4	–
11	∥	8.56	2.1 ± 0.7	–	–

a) Ref. [8]: $D_{NMR} = 0.25 \times 10^{-14}$ m^2 s^{-1} at 300 K.

to the c axis we have taken $a = 4.15$ Å and $g = 2/3$. As can be seen from table 2, there is satisfactory agreement between the diffusion coefficients calculated from ^{19}F NMR relaxation data, and those calculated from ionic conductivity data. The D_{NMR} value 0.25×10^{-14} m^2 s^{-1} for D_{NMR} at 300 K of pure LaF_3 as reported by Sher et al. [8], fits well with the D_σ and D_{NMR} values given in table 2. Furthermore, the agreement between D_σ and D_{NMR} indicates the absence of associates $(Ba_{La}V_F)^X$ in $La_{1-x}Ba_xF_{3-x}$ above room temperature, because generally these would bring about a much lower D_σ than D_{NMR}.

For the conductivity region above 415 K, the exchange mode, the pre-exponential factor, σ_2^0, can be given by

$$\sigma_2^0 = [V_F^\bullet] q^2 a^2 \nu_0 g/k \exp(\Delta S_m/k) . \qquad (10)$$

With eq. (10) we can calculate the entropy of migration if we know the concentration of fluoride vacancies $[V_F^\bullet]$.

It will be obvious that for pure LaF_3 we can make a good estimation of the number of fluoride ion vacancies for $T > 300$ K by using the concentration of 0.06 m/o of dipoles as determined by dielectric relaxation measurements at low temperatures [27]. For the doped samples the concentration of fluoride ion vacancies is approximated by the dopant concentration as determined by the analysis. We have calculated the entropy of migration using the following values: $a = 2.5$ Å and $g = 2$ (see table 2). This table shows that ΔS_m becomes more negative on going from the pure to the doped materials. There appears only a slight tendency to decrease further for high solute content. The entropy of migration results from changes in lattice vibrational modes during the jumping process. The numerical values for ΔS_m in table 2 reveal that in the fluoride ion vacancy jump process the entropy is lowered with increasing x.

The intrinsic point defects in LaF_3 are thermally generated according to a Schottky mechanism: $La_{La}^X + 3F_F^X + V_{La}''' + 3V_F^\bullet \rightleftharpoons (LaF_3)_{def.}$. The general relation governing the ionic conductivity in the intrinsic region of LaF_3 is given by

$$\sigma T = \sqrt[4]{\tfrac{1}{3}} N q^2 a^2 \nu_0 g/k \exp(\Delta S_f/4 + \Delta S_m)/k$$

$$\times \exp(-\Delta H_f/4 + \Delta H_m)/kT , \qquad (11)$$

here ΔS_f and ΔH_f denote the formation entropy and enthalpy of a Schottky defect quartet, respectively. With the pre-exponential factor of the intrinsic conductivity region of undoped LaF_3, and the entropy of migration (table 2), we can determine the entropy of formation. Assuming $a = 2.5$ Å and $g = 2$, it appears that $\Delta S_f/4k$ has the value 3.6 ± 1.4.

The vibrational frequencies of a solid are affected by the formation of lattice defects. The general equation which relates the entropy to the lattice vibration frequencies is in the case of vacancies to a first

approximation given (following ref. [35]) by

$$\exp(\Delta S/k) = (\nu_0/\nu)^X \ , \qquad (12)$$

where ν_0 is equal to the Debye frequency, and ν is the vibrational frequency of the lattice perturbed by a vacancy. X denotes the coordination number of ions adjacent to the vacancy. If we assume that the fluoride ion vacancies affect the entropy of the crystal by changing the vibrational frequencies of the nearest lanthanum ions only, i.e.

$$S(V_F^{\bullet}) = x_{V_F^{\bullet}} k \ln(\nu_0/\nu_{V_{La}^{'''}}) \ , \qquad (13)$$

and that the lanthanum ion vacancies affect the vibrational frequencies of the adjacent fluoride ions only, i.e.

$$S(V_{La}^{'''}) = x_{V_{La}^{'''}} k \ln(\nu_0/\nu_{V_F^{\bullet}}) \ , \qquad (14)$$

we can calculate with $\Delta S_f/k = 3.6$

$$\nu_0^2 = 1.4 \nu_{V_F^{\bullet}} \nu_{V_{La}^{'''}} \ . \qquad (15)$$

The lanthanum ions are surrounded by at most 11 fluoride ions, and the fluoride ions are surrounded either by 3 or 4 lanthanum ions [9]. Eq. (15) was calculated assuming a weighted average coordination number of 3.67.

With the entropy of migration as calculated before ($\Delta S_m/k = -1.5$), we can determine approximately the frequency of the nearest-neighbour vibrations taking into account the weighted average coordination of 3.67

$$S(V_F^{\bullet}) = k \ln(\nu_0/\nu_{V_{La}^{'''}})^{3.67} \ . \qquad (16)$$

We assume here, that the entropy of migration (ΔS_m) represents the entropy of the saddle point between the equilibrium states of the entropy of formation (ΔS_f). On behalf of this simple model [36], we obtain from eqs. (15) and (16)

$$\nu_{V_{La}^{'''}} > \nu_0 \quad \text{and} \quad \nu_{V_F^{\bullet}} < \nu_0 \ ,$$

with $\nu_{V_F^{\bullet}} \nu_{V_{La}^{'''}} < \nu_0^2$.

This is in accordance with Kröger's [35] general assessment that $\nu < \nu_0$ should hold. Since vacancy formation implies that ions near the vacancies are bound with fewer bonds than ions in the unperturbed lattice, we might expect overall decreased vibrational frequencies.

Acknowledgement

The authors are grateful to Professor G. Blasse for his criticism during the preparation of the manuscript. Thanks are due to Mr. M. de Bruin of the Interuniversity Reactor Institute, Delft, for the neutron activation analysis. We are indebted to Dr. D.R. Franceschetti (Memphis State University), Dr. A.K. Cheetham (University of Oxford) and Professor H. Schulz (MPI-Stuttgart) for making their data available prior to publication.

References

[1] T.N. Rezukhina, T.F. Sisoeva, L.I. Holokhonova and E.G. Ippolitov, J. Chem. Thermodynamics 6 (1974) 883.
[2] B.C. LaRoy, A.C. Lilly and C.O. Tiller, J. Electrochem. Soc. 120 (1973) 1668.
[3] M. Frant and J. Ross, Science 154 (1966) 1553.
[4] T.A. Fjeldly and K. Nagy, J. Electrochem. Soc. 127 (1980) 1299.
[5] D.R. Figueroa, A.V. Chadwick and J.H. Strange, J. Phys. C11 (1978) 55.
[6] K.E.D. Wapenaar, J.L. van Koesveld and J. Schoonman, Solid State Ionics 2 (1981) 145.
[7] L.E. Nagel and M. O'Keeffe, in: Fast ion transport in solids, ed. W. van Gool (North-Holland, Amsterdam, 1973) p. 165.
[8] A. Sher, R. Solomon, K. Lee and M.W. Muller, Phys. Rev. 144 (1966) 593.
[9] W.L. Fielder, Nasa-Tech. Notes D 5505 (1969).
[10] A.V. Chadwick, D.S. Hope, G. Jaroszkiewicz and J.H. Strange, in: Fast ion transport in solids, eds. P. Vashishta, J.N. Mundy and G.K. Shenoy (North-Holland, Amsterdam, 1979) p. 683.
[11] J. Schoonman, G. Oversluizen and K.E.D. Wapenaar, Solid State Ionics 1 (1980) 211.
[12] J.R. Igel, M.C. Wintersgill, J.J. Fontanella, A.V. Chadwick, C.G. Andeen and V.E. Bean, J. Phys. C15 (1982) 7215.
[13] Gmelin Handbuch der Anorganischen Chemie, Seltenerdelemente, Teil C3. Sc, Y, La and Lanthanide, 8th Ed. (Springer, Berlin, 1976) pp. 50–58; 98–100; 158–161.
[14] B. Maximov and H. Schulz, Acta Cryst. B., to be published.
[15] A. Roos, Mat. Res. Bull. 18 (1983) 405.
[16] A. Roos, D.R. Franceschetti and J. Schoonman, J. Phys. Chem. Solids, to be published.
[17] K. Schlyter, Arkiv. Kemi 5 (1952) 73.
[18] M. Mansmann, Z. Kristallogr. 122 (1965) 399.

[19] A. Zalkin, D.H. Templeton and T.E. Hopkins, Inorg. Chem. 5 (1966) 1466.
[20] A.K. Cheetham, B.E. Fender, H. Fuess and A.F. Wright, Acta Cryst. B32 (1976) 94.
[21] K. Lee and A. Sher, Phys. Rev. Letters 14 (1965) 1027.
[22] A.K. Cheetham, University of Oxford, unpublished results.
[23] G.A. Jaroszkiewicz and J.H. Strange, J. Phys. (Paris) C6 (1980) 246.
[24] A. Roos, A.F. Aalders, J. Schoonman, A.F.M. Arts and H.W. de Wijn, Solid State Ionics 9/10 (1983) 571.
[25] A.F. Aalders, A. Polman, A.F.M. Arts and H.W. de Wijn, Solid State Ionics 9/10 (1983) 539.
[26] M. Goldman and L. Shen, Phys. Rev. 144 (1966) 321.
[27] A. Roos, M. Buijs, K.E.D. Wapenaar and J. Schoonman, J. Phys. Chem. Solids, to be published.
[28] D.R. Franceschetti and P.C. Shipe, Solid State Ionics 11 (1984) 285.
[29] J.A. Kilner and C.D. Waters, Solid State Ionics 6 (1982) 253.
[30] A.B. Lidiard, Handbuch der Physik, ed. S. Flügge (Springer, Berlin, 1957) p. 246.
[31] A. Nakamura and J. Bruce Wagner Jr., J. Electrochem. Soc. 127 (1980) 2325.
[32] G. Khachaturyan and B.I. Pokrovskii, Sov. Phys. Crystallogr. 25 (1980) 344.
[33] G.E. Pike, W.J. Camp, C.H. Seager and G.L. McVay, Phys. Rev. B10 (1974) 4909.
[34] V.K. Shante and S. Kirkpatrick, Adv. Phys. 20 (1971) 325.
[35] F.A. Kröger, The chemistry of imperfect crystals, 2nd Rev. Ed., Vol. 2 (North-Holland, Amsterdam, 1974) p. 151.
[36] J. Schoonman, J. Solid State Chem. 4 (1972) 466.
[37] T.S. Light and C.C. Cappuccino, J. Chem. Educ. 52 (1975) 247.
[38] K.E.D. Wapenaar and J. Schoonman, J. Electrochem. Soc. 126 (1979) 667.
[39] T. Takahashi, H. Iwahara and T. Ishikawa, J. Electrochem. Soc. 124 (1977) 280.
[40] B.P. Sobolev and N.L. Tkachenko, Sov. Phys. Crystallogr. 20 (1976) 728.